PULSAR RADIO EMISSION ALTITUDE FROM CURVATURE RADIATION

R. T. Gangadhara

Indian Institute of Astrophysics, Bangalore – 560034, India

ganga@iiap.res.in

ABSTRACT

We assume that the relativistic sources moving along the dipolar magnetic field lines emit curvature radiation. The beamed emission occurs in the direction of tangents to the field lines, and to receive it, the sight line must align with the tangent within the beaming angle $1/\gamma$, where γ is the particle Lorentz factor. By solving the viewing geometry in an inclined and rotating dipole magnetic field, we show that, at any given pulse phase, observer tends to receive radiation only from the specific heights allowed by the geometry. We find outer conal components are emitted at higher altitudes compared to inner components including the core. At any pulse phase, low frequency emission comes from higher altitudes than high frequency emission. We have modeled the emission heights of pulse components of PSR B0329+54, and estimated field line curvature radii and particle Lorentz factors in the emission regions.

Subject headings: stars: magnetic fields — radio continuum: stars — pulsars: individual (PSR B0329+54) — pulsars: general

1. INTRODUCTION

Pulsar radio emission is generally thought to be coherent radiation from the relativistic plasma streaming along the open magnetic field lines. The emission beam geometry has been widely attempted to interpret in terms of emission in purely dipolar magnetic field (e.g., Radhakrishnan & Cooke 1969; Goldreich & Julian 1969; Sturrock 1971; Ruderman & Sutherland 1975; Michel 1982; Blaskiewicz et al. 1991).

Radhakrishnan and Cooke (1969) have proposed the rotating vector model (RVM) to explain the polarization-angle (PA) traverse (S-curve) of pulsar profiles. It has been fitted to average PA curves, and found to be quite successful (e.g., Lyne & Manchester 1988). The

three chief assumptions (Hibschman & Arons 2001) of RVM model are (i) the relativistic plasma flow is collimated by strong dipolar magnetic field lines, (ii) the observed radiation is beamed in the direction of tangents to the field lines, and (iii) the polarization angle is at a fixed angle to the curvature of field lines, as is the case of vacuum curvature radiation. Based on the assumptions (i) and (ii), we have attempted to locate the radio emission region in pulsar magnetosphere from which a distant observer receives the radiation.

Statistical analysis of the distribution of pulse components within the pulse window indicates that the emission beam is conal (e.g., Mitra & Deshpande 1999; Kijak & Gil 2002). Rankin (1993) has indicated that inner pulse components are emitted at lower altitudes than the outer ones. Gangadhara and Gupta (2001, hereafter GG01) have estimated the emission height of different radio pulse components of PSR B0329+54, based on the aberration-retardation phase shift. They have also found that the inner components of pulse profiles originate from lower altitudes than the outer components. In the following paper Gupta and Gangadhara (2003) have then estimated the emission heights of 6 more pulsars using the same technique. Recently, the emission heights of all those pulsars have been re-estimated by Dyks, Rudak and Harding (2003, hereafter DRH03) by revising the aberration phase–shift relation given in GG01. Also, there are other claims for core and cone emission altitudes being different (e.g., Mitra & Rankin 2002) and roughly the same (e.g., Gil 1991).

In this paper, we solve the viewing geometry for receiving the radio waves by a distant observer in § 2. By assuming the particle Lorentz factors, we show in § 2.2 that curvature radiation predicts the emission heights which are comparable to the radio emission heights in PSR B0329+54. In § 3, by utilizing the properties of curvature radiation and the emission altitudes estimated from aberration–retardation phase shift (DRH03), we estimate the field line curvature radii and particle Lorentz factors in the emission region.

2. EMISSION–BEAM GEOMETRY

Consider a magnetic dipole situated at the origin with magnetic dipole moment ($\hat{\mathbf{m}}$) aligned with the rotation axis ($\hat{\mathbf{\Omega}}$). In polar coordinates, the equation for a dipole–field line (Alfvén & Falthämmar 1963) is $r = r_{\rm e} \sin^2\theta$, where θ is the magnetic colatitude and r the distance from the origin. The parameter $r_{\rm e}$ is the *field line constant*, which is a distance from origin to the point of field line intersection with the equatorial plane ($\theta = \pi/2$). In the case of an aligned dipole, $r_{\rm e} = r_{\rm LC}$ for the last open field line, where $r_{\rm LC} = Pc/2\pi$ is the light cylinder radius, c the speed of light, and P the pulsar period. In the Cartesian coordinate system with z-axis parallel to $\hat{\mathbf{\Omega}}$, the position vector of an arbitrary point Q on a field line

is given by

$$\mathbf{r}_{\rm c} = r_{\rm e}(\sin^3\theta\cos\phi,\, \sin^3\theta\sin\phi,\, \sin^2\theta\cos\theta), \tag{1}$$

where ϕ is the magnetic azimuth.

Now consider the situation where the dipole ($\hat{\mathbf{m}}$) is *inclined* through an angle α with respect to $\hat{\mathbf{\Omega}}$, and *rotated* by phase ϕ' around z-axis, as shown in Figure 1. The position vector of the point Q on a magnetic field line, which is tilted and rotated, is given by

$$\mathbf{r}_{\rm ct} = \Lambda \cdot \mathbf{r}_{\rm c} \quad , \tag{2}$$

where the transformation matrix $\Lambda = R \cdot I$. The matrices for tilt (inclination) I and rotation $\mathbf{R}$ are given by

$$I = \begin{pmatrix} \cos\alpha & 0 & \sin\alpha \\ 0 & 1 & 0 \\ -\sin\alpha & 0 & \cos\alpha \end{pmatrix} , \quad R \;=\; \begin{pmatrix} \cos\phi' & -\sin\phi' & 0 \\ \sin\phi' & \cos\phi' & 0 \\ 0 & 0 & 1 \end{pmatrix} . \tag{3}$$

The matrix I produces clockwise rotation of the dipole around y-axis, and R counter-clockwise rotation around the z-axis.

At Q, we find the *tangent* to the field line by evaluating $\mathbf{b}_{\rm t} = \partial\mathbf{r}_{\rm ct}/\partial\theta$, and the *curvature* by evaluating $\mathbf{k}_{\rm t} = d\hat{\mathbf{b}}_{\rm t}/ds$, where $\hat{\mathbf{b}}_{\rm t} = \mathbf{b}_{\rm t}/|\mathbf{b}_{\rm t}|$ is a unit tangent vector, ds is the arc length of the field line and $|\mathbf{b}_t| = r_{\rm e}\,\sqrt{5+3\,\cos(2\,\theta)}\,\sin\theta/\sqrt{2}$. Therefore, the field line curvature radius is given by

$$\rho = \frac{1}{|\mathbf{k}_{\rm t}|} = \frac{r_{\rm e}\sin\theta\,[5+3\cos(2\,\theta)]^{3/2}}{3\sqrt{2}\,[3+\cos(2\,\theta)]}. \tag{4}$$

Since $\hat{\mathbf{m}}$ is chosen to be parallel to $\hat{\mathbf{z}}$, the transformed magnetic dipole moment is given by

$$\hat{\mathbf{m}}_{\rm t} = \Lambda \,\cdot\, \hat{\mathbf{z}} = (\sin\alpha\,\cos\phi',\, \sin\alpha\,\sin\phi',\, \cos\alpha). \tag{5}$$

Hence the magnetic field of a dipole (Jackson 1975), which is inclined and rotated, is given by

$$\mathbf{B}_{\rm t} = B_0\left(\frac{r_{NS}}{r}\right)^3 \left[3\,(\hat{\mathbf{r}}\cdot\hat{\mathbf{m}}_{\rm t})\,\hat{\mathbf{r}} - \hat{\mathbf{m}}_{\rm t}\right], \tag{6}$$

where B_0 is the surface magnetic field and $r_{\rm NS} \sim 10$ km is the neutron star radius. It can be easily shown that $\mathbf{B}_{\rm t}$ satisfies $\nabla\cdot\mathbf{B}_{\rm t} = 0$.

The dominant magnetic field in the emission region is often shown to be consistent with being dipolar and to study the shape of pulsar radio beams (e.g., Narayan & Vivekanand 1983; Lyne & Manchester 1988; Kramer et al. 1997). In a static dipole magnetic field approximation, the basic features of the pulsar magnetosphere can be understood. On the time scales of the order of pulse-phase bin, which is very small compared to the pulsar period, the rotating dipole may be treated, approximately, a static dipole.

2.1. *Magnetic Colatitude and Azimuth of Emission Spot*

Consider the sight line $\hat{\mathbf{n}} = (\sin\zeta,\ 0,\ \cos\zeta\ )$, which lies in the xz–plane and makes an angle ζ with respect to $\hat{\mathbf{\Omega}}$, where $\zeta = \alpha + \beta$, and β is the angle of closest approach of sight line with respect to the magnetic axis. The half opening angle (Γ) of the emission beam is given by

$$\cos\Gamma = \hat{\mathbf{n}} \cdot \hat{\mathbf{m}}_{\rm t} = \cos\alpha\cos\zeta + \sin\alpha\ \sin\zeta\ \cos\phi' \ . \tag{7}$$

If τ is the angle between $\hat{\mathbf{b}}_{\rm t}$ and $\hat{\mathbf{m}}_{\rm t}$ then we have

$$\cos\tau = \hat{\mathbf{b}}_{\rm t} \cdot \hat{\mathbf{m}}_{\rm t} = \frac{1 + 3\ \cos(2\,\theta)}{\sqrt{10 + 6\ \cos(2\,\theta)}} \, . \tag{8}$$

In relativistic flow, radiation is beamed in the direction of field line tangent. So, at any instant, observable radiation comes from a spot in the magnetosphere where the tangent vector $\hat{\mathbf{b}}_{\rm t}$ points in the direction of $\hat{\mathbf{n}}$. That is $\Gamma \approx \tau$ at the emission spot. Therefore, using equations (7) and (8), we can find the relation for *magnetic colatitude* θ as a function of Γ :

$$\cos(2\,\theta) = \frac{1}{3}(\cos\Gamma\,\sqrt{8 + \cos^2\Gamma} - \sin^2\Gamma) \, , \qquad -\pi \le \Gamma \le \pi \, . \tag{9}$$

This equation is similar to the one given in GG01 (see, eq. 4) for θ. However, the equation (9) is superior compared to GG01's equation as it represents a single physical solution when Γ changes sign. For $\Gamma \ll 1$, equation (9) reduces to the well known approximate form $\theta \approx \frac{2}{3}\Gamma$.

Next, let κ be the angle between $\hat{\mathbf{n}}$ and $\hat{\mathbf{b}}_{\rm t}$, then we have

$$\begin{aligned} \cos\kappa &= \hat{\mathbf{n}} \cdot \hat{\mathbf{b}}_{\rm t} \\ &= \cos^2\Gamma + (\cos\alpha\ \sin\zeta\ \cos\phi' - \sin\alpha\ \cos\zeta)\ \sin\Gamma\cos\phi - \sin\zeta\ \sin\phi'\sin\Gamma\sin\phi. \end{aligned} \tag{10}$$

Again to receive the radiation $\kappa \sim 0$, therefore, we find the *magnetic azimuth* ϕ of the emission spot by solving $\hat{\mathbf{n}} \cdot \hat{\mathbf{b}}_{\rm t} = 1$ and $\hat{\mathbf{n}} \times \hat{\mathbf{b}}_t = 0$:

$$\begin{aligned} \sin\phi &= -\sin\zeta\ \sin\phi'\csc\Gamma, \\ \cos\phi &= (\cos\alpha\ \sin\zeta\ \cos\phi' - \cos\zeta\ \sin\alpha)\csc\Gamma. \end{aligned}$$

Therefore, we have

$$\phi = \arctan\left(\frac{\sin\zeta\ \sin\phi'}{\cos\zeta\ \sin\alpha - \cos\alpha\ \sin\zeta\ \cos\phi'}\right). \tag{11}$$

Note that ϕ is measured with respect to the meridional plane defined by $\hat{\mathbf{\Omega}}$ and $\hat{\mathbf{m}}_{\rm t}$.

2.2. *Radio Emission Height*

Pulsar radio emission is generally believed to be coherent curvature radiation by secondary pair plasma streaming along the dipolar magnetic field lines. The characteristic frequency of curvature radiation, at which the emission peaks, is given by (Ruderman & Sutherland 1975):

$$\nu = \frac{3c}{4\pi}\frac{\gamma^3}{\rho}, \tag{12}$$

where γ and ρ are the Lorentz factor and the radius of curvature of trajectory of a relativistic particle, respectively. Since particles closely follow the curved dipolar field lines, the curvature of particle trajectory can be approximated with the curvature of field lines.

For the given ν and γ, equation (12) predicts the value of ρ required. Then using equation (4) we can find the field line constant $r_{\rm e}$ with the help of $\theta_{\rm em}$ obtained from equation (9). The azimuth $\phi_{\rm em}$ of the emission spot can be determined by using equation (11). Hence, by having defined $(r_{\rm e}, \theta_{\rm em}, \phi_{\rm em})$, we can estimate the emission height $r_{\rm em}$ of radio waves of frequency ν with respect to pulse phase ϕ' using equation (2).

Based on the aberration-retardation phase-shift of pulse components in observed profiles, Gangadhara and Gupta (2001) have estimated the emission heights of pulse components in PSR B0329+54 at frequencies 325 MHz and 606 MHz. Recently, Dyks, Rudak and Harding (2003) have revised the aberration phase–shift relation given in GG01, and re-estimated the emission heights. In Figure 2, we have plotted the revised emission heights (marked points with error bars).

For modeling the emission heights in PSR B0329+54, we adopt $(\alpha, \beta) = (30^\circ, 2.1^\circ)$ given by Rankin (1993). We find that the curvature emission predicts the emission heights (solid and dashed line curves in Figure 2) which are comparable to the observed ones (DRH03) if the secondary particle Lorentz factor $\gamma \approx 340$ and 390 for the emissions at 325 MHz and 606 MHz, respectively. Figure 2 shows that at any given frequency the emission near the pulse center (core) comes from lower heights compared to outer conal components, in agreement with the results derived from observations (marked points). At any pulse phase, low frequency emission comes from higher altitude than the high frequency emission, in agreement with the well known radius–to–frequency mapping (RFM) (e.g., Cordes 1978; Phillips 1992). We find RFM mapping is not uniform across the pulse window, i.e., it is more pronounced in the case of outer cons (say, cones 3 & 4) than in the inner cones (say, cones 1 & 2). Mitra and Rankin (2002) have also made a similar proposition from the study of 10 selected pulsars. The emission height difference $\delta r_{\rm em}$ between the two frequencies increase progressively with respect to pulse phase, and the marked points in Figure 2 indicate $\delta r_{\rm em} \approx 14 + 0.046\,\phi'^{\,2} + 0.003\,\phi'^{\,4}$ km, where the pulse phase ϕ' is in degrees.

2.3. *The Polar Cap*

The polar cap boundary is defined by the last open field lines for which $\mathbf{k}_t \cdot \hat{\mathbf{z}} = 0$ at the light cylinder. Therefore, the magnetic colatitude $\theta_{\rm lof} = \theta$, at which $\mathbf{k}_{\rm t} \cdot \hat{\mathbf{z}}$ vanishes, is given by

$$\cos(2\,\theta_{\rm lof}) = \frac{-3\,{a_1}^2 - a_2\,\sqrt{8\,{a_1}^2 + {a_2}^2}}{9\,{a_1}^2 + {a_2}^2}\,, \qquad -\frac{\pi}{2} < \phi \leq \frac{\pi}{2} \tag{13}$$

where $a_1 = \sin\alpha\,\cos\phi$ and $a_2 = 3\,\cos\alpha$. Next, for the range of $\pi/2 < \phi \leq 3\pi/2$, the colatitude is given by $\pi - \theta_{\rm lof}$. The angle (η) between $\hat{\mathbf{r}}_{\rm ct}$ and $\hat{\mathbf{z}}$ is given by

$$\cos\eta = \hat{\mathbf{z}} \cdot \hat{\mathbf{r}}_{\rm ct} = \cos\alpha\,\cos\theta - \sin\alpha\,\sin\theta\,\cos\phi. \tag{14}$$

If $\eta_{\rm lof} = \eta$ at the light cylinder for last open field line then we have $|\mathbf{r}_{\rm ct}|\sin\eta_{\rm lof} = r_{\rm LC}$, and the last open field line constant

$$r_{\rm e,lof} = r_{\rm LC}\,\csc^2\theta_{\rm lof}\,\csc\eta_{\rm lof}\,. \tag{15}$$

Hence the radial position of foot of a last open field line from the magnetic axis is given by

$$s_{\rm p} = r_{\rm NS}\theta_{\rm p}, \tag{16}$$

where $\theta_{\rm p} = \arcsin(\sqrt{r_{\rm NS}/r_{\rm e,lof}})$ is the colatitude of foot of last open field line.

To plot polar cap consider the Cartesian coordinate system: ($\rm x_B$, $\rm y_B$, $\rm z_B$) such that the axis $\rm z_B$ is parallel to $\hat{\mathbf{m}}_{\rm t}$ and $\rm x_B$ lies in the meridional plane. The coordinates of foot of a last open field line is given by

$$(x_{\rm B}\,, y_{\rm B}) = (s_{\rm p}\cos\phi\,, s_{\rm p}\sin\phi). \tag{17}$$

Using $\alpha = 30^\circ$, the polar cap of PSR B0329+54 is plotted in Figure 3. It is nearly elliptical with the dimension of 164 m in the $\rm x_B$ direction and 171 m in the direction of $\rm y_B$, in agreement with the polar cap shapes proposed by Biggs (1990).

For a given pulse phase ϕ', using equations (9) and (11), we can find $\theta_{\rm em}$ and $\phi_{\rm em}$ of the emission spot. The radial location of foot of field lines, from which a distant observer receives the radiation, is given by

$$s_{\rm em} = \sqrt{\frac{r_{\rm NS}^3}{r_{\rm em}}}\sin\theta_{\rm em}. \tag{18}$$

Thus, by knowing $s_{\rm em}$ and $\phi_{\rm em}$ one can specify ($x_{\rm B}$, $y_{\rm B}$) of the foot of field lines, which direct the radiation beam towards the observer. The values of $s_{\rm em}$ estimated from the

conal aberration-retardation phase-shift (marked points with error bars in $s_{\rm em}$) are plotted in Figure 3. The model (dashed and solid line) curves represent the locus of foot of those field lines, which are accessible to a distant observer in 325 MHz and 606 MHz observations, respectively. We find the low frequency emission is received from the field lines which lie closer to the magnetic axis than the high frequency ones. The curve (solid line) indicates increasing conal ring spacing ($\delta s_{\rm em}$) between the successive rings from inner (cone 1) to outer (cone 4) on polar cap: ~ 14 m between the $1^{\rm st}$ ring and the $2^{\rm st}$ ring, 16 m between $2^{\rm nd}$ and $3^{\rm rd}$, and 19 m between $3^{\rm rd}$ and $4^{\rm th}$. The dashed line curve for 325 MHz emission also indicate the similar ring spacings, except they are less by ~ 0.5 m. These results tend to support the model of concentric rings of sparks produced in the vacuum gap region just above the neutron surface (e.g., Ruderman & Sutherland 1975; Gil & Sendyk 2000).

3. DISCUSSION

In the previous section, to explain the emission height of components in PSR B0329+54, we selected the Lorentz factor γ of about 340 and 390 for the emissions at 325 MHz and 606 MHz, respectively. It means ρ and γ assume constant values across the pulse window. However, it may not be reality, as the model heights significantly depart from the observed ones (marked points) as indicated by Figure 2. On other hand, one can turn around the calculation by accepting the observed emission heights ask for the required γ and ρ. In column 2 of Tables 1 & 2, we have given the phase location of conal components in the absence of aberration-retardation phase shift (see, eq. 11, GG01), i.e., in corotating frame. Next, the columns 3 and 4 give the magnetic colatitude θ and the longitude ϕ of emission spot, estimated using equations (9) and (11). The small values of $\theta < 6^\circ$ implies the conal emission mostly comes from the vicinity of magnetic axis. By having known $r_{\rm em}$ and $\theta_{\rm em}$, we estimated the radius of curvature ρ using equation (4), and given in column 5. It shows inner cones are emitted from the region of smaller curvature than outer ones. Next, for a given frequency ν and known ρ, equation (12) allows to estimate the γ of secondary particles, as given in column 6. It shows particles with slightly higher γ move on the field lines associated with outer cones than inner ones.

The emission beam by relativistic particles is centered on their velocity, which is roughly parallel to the field line tangent $\hat{\mathbf{b}}_{\rm t}$, and has a radial angular width of $1/\gamma$. Consequently, observer tends to receive the radiation even when $\hat{\mathbf{n}}$ does not perfectly align with $\hat{\mathbf{b}}_{\rm t}$, which can lead to a spread in the emission height as well as in pulse phase of component peak location. So, we estimated the spread in emission height of conal components by allowing Γ in equation (9) to vary by $1/\gamma$. However, we find the spread is minimal and lies within

the error bars. For example, at 325 MHz, we find 9 km for the 1st cone and 15 km for the 4th cone. At 606 MHz, it is 6 km for the 1st cone and 10 km for the 4th. For other cones the spread lies in between these values. We also estimated the spread in phase of component peaks, and found to be less than 0.4° for all the components. If we compare the emission heights (DRH03) along with these spreads, we find the emission regions of conal components at the two frequencies are well separated: it is 14 km in the case of 1st and 214 km for the 4th. Further, the pulse phase locations of conal components are different at the two frequencies, as indicated by column 2 in Tables 1 & 2. So, the observer tends to see the components separated in phase as well. Note that the received radiation is maximum only when $\hat{\mathbf{n}}$ perfectly aligns with $\hat{\mathbf{b}}_{\rm t}$. Hence we may conclude that the observer tends to receive the radiation at the two frequencies from two distinctly located regions in the magnetosphere.

Using these values of γ and ρ, we estimated the power radiated by an electron or a positron by curvature emission (see, eq. 25a, Ruderman & Sutherland 1975), and given in column 7. It shows the single particle emission is maximum in the region of inner cone than in the outer cone regions. However, we know from the estimates made by Ruderman and Sutherland (1975) that the incoherent superposition of single particle radiation cannot explain the pulsar radio emission. The very high brightness temperature (10^{25}–10^{30} K) of pulsars lead to the conclusion that it must be coherent. The coherence due to the bunching of plasma particles in the magnetosphere was proposed much earlier (e.g., Pacini & Rees 1970; Sturrock 1971). The coherence due to bunching goes as inverse of wavelength of radio waves, therefore, the emission by bunches at low frequency tends to dominate the high frequency emission.

Thus, we have developed a method for estimating the possible values of γ and ρ needed for the emission of radio waves at a given frequency. By matching the coherent curvature emission with the observed pulsar fluxes, one may be able to estimate the plasma density and the coherency (bunching) factor exist in the radio emission region of pulsars. For $\nu \geq \nu_p$ strong coherent radiation occurs, where $\nu_{\rm p}$ is the plasma frequency (Ruderman & Sutherland 1975).

While estimating the aberration-retardation phase shift of conal components, the core (reference) phase was set to zero (GG01; DRH03). However, it is possible that the core is also emitted at a finite height from the neutron star surface, as indicated by Figure 2. We fitted a 4th degree polynomial to the emission heights (marked points in Fig. 2) of 8 conal components. At zero phase, the fit indicated emission height of 26 ± 50 km for the 325 MHz points and 12 ± 45 km for the 606 MHz points. These heights may be treated as minimum values for the core emission height, as the component heights themselves have been estimated by setting the core phase to zero. Though it is important to consider the emission height

of core, we believe our results will not change significantly by the core height, as aberration and retardation are minimal at that height.

4. CONCLUSION

By assuming the curvature emission by relativistic sources is beamed in the direction of tangent to the dipolar magnetic field lines, we have resolved the pulsar radio emission geometry by solving the viewing geometry in an inclined and rotating dipolar magnetic field. Due to the geometric restrictions, a distant observer tends to receive outer conal components from higher altitudes than inner ones including the core. Further, we find low frequency emission comes from higher altitudes than high frequency emission, in agreement with the radius-to-frequency mapping (RFM). We find RFM is more pronounced in the outer conal components than in the inner ones. Using the emission heights obtained from aberration-retardation phase shift, we have estimated the probable values of Lorentz factor and field line curvature radii in the emission region.

I would like to thank Don Melrose and Simon Johnston for illuminating discussions, and J. M. Rankin, J. A. Gil, Y. Gupta, V. Krishan, and C. Sivaram for comments. I thank anonymous referee for useful comments.

REFERENCES

Alfvén, H., Falthämmar, C. -G. 1963, Cosmical Electrodynamics, Oxford Univ. Press, London, p 4

Biggs, J. D. 1990, MNRAS, 245, 514

Blaskiewicz, M., Cordes, J. M., & Wasserman, I. 1991, ApJ, 370, 643

Cordes, J. M. 1978, ApJ, 222, 1006

Dyks, J., Rudak, B., & Harding, A. K. 2003, ApJ, in press (astro-ph/0307251) (DRH03)

Gangadhara, R. T., & Gupta, Y. 2001, ApJ, 555, 31 (GG01)

Gil, J. A. 1991, A&A, 243, 219

Gil, J. A., & Sendyk, M. 2000, ApJ, 541, 351

Goldreich, P., & Julian, W. H. 1969, ApJ, 157, 869

Gupta, Y., & Gangadhara, R. T. 2003, ApJ, 584, 418

Hibschman, J. A., & Arons, J. 2001, ApJ, 546, 382

Jackson, J. D., 1975, Classical Electrodynamics, John Wiley & Sons, Inc., New York, Second U.S. Edition, p 182

Kijak, J., & Gil., J. 2002, A&A, 392, 189

Kramer, M., et al., 1997, A&A, 322, 846

Lyne, A. G., & Manchester, R. N. 1988, MNRAS, 234, 477

Michel, F. C. 1982, Rev. Mod. Phys., 54, 1

Mitra, D., & Deshpande, A. A. 1999, A&A, 346, 906

Mitra, D., & Rankin, J. M. 2002, ApJ, 577, 322

Narayan, R., & Vivekanand, M. 1983, A&A, 122,45

Pacini, F., & Rees, M. J. 1970, Nat., 226, 622

Phillips, J. A. 1992, ApJ, 385, 282

Radhakrishnan, V., & Cooke, D. J. 1969, Astrophys. Lett., 3, 225

Rankin, J. M. 1993, ApJ, 405, 285

Ruderman, M. A., & Sutherland, P. G. 1975, ApJ, 196, 51

Sturrock, P. A. 1971, ApJ, 164, 229

Table 1: Parameters related to radio emission from PSR B0329+54 at 325 MHz

Cone No.	ϕ' (deg)	θ (deg)	ϕ (deg)	$\rho/r_{\rm LC}$	γ	P/P_1[†]
1	5.0 ± 0.26	2.22 ± 0.07	-53.0 ± 1.6	0.15 ± 0.00	286 ± 3	1.00 ± 0.08
2	8.4 ± 0.19	3.21 ± 0.06	-67.8 ± 0.6	0.23 ± 0.00	329 ± 2	0.76 ± 0.03
3	12.0 ± 0.27	4.35 ± 0.09	-76.5 ± 0.5	0.31 ± 0.01	363 ± 2	0.62 ± 0.03
4	17.0 ± 0.80	5.99 ± 0.26	-83.9 ± 1.0	0.33 ± 0.01	370 ± 5	0.60 ± 0.06

[†] $P_1 = 1.16 \times 10^{-16}$ erg s^{-1}

Table 2: Parameters related to radio emission from PSR B0329+54 at 606 MHz

Cone No.	ϕ' (deg)	θ (deg)	ϕ (deg)	$\rho/r_{\rm LC}$	γ	P/P_1[†]
1	4.9 ± 0.25	2.19 ± 0.07	-52.4 ± 1.6	0.12 ± 0.00	328 ± 3	1.00 ± 0.07
2	7.8 ± 0.18	3.02 ± 0.06	-65.8 ± 0.6	0.21 ± 0.00	391 ± 2	0.70 ± 0.03
3	11.0 ± 0.45	4.02 ± 0.14	-74.5 ± 1.0	0.26 ± 0.01	419 ± 5	0.61 ± 0.05
4	15.7 ± 0.59	5.56 ± 0.19	-82.3 ± 0.8	0.26 ± 0.01	420 ± 5	0.61 ± 0.05

[†] $P_1 = 3.06 \times 10^{-16}$ erg s^{-1}

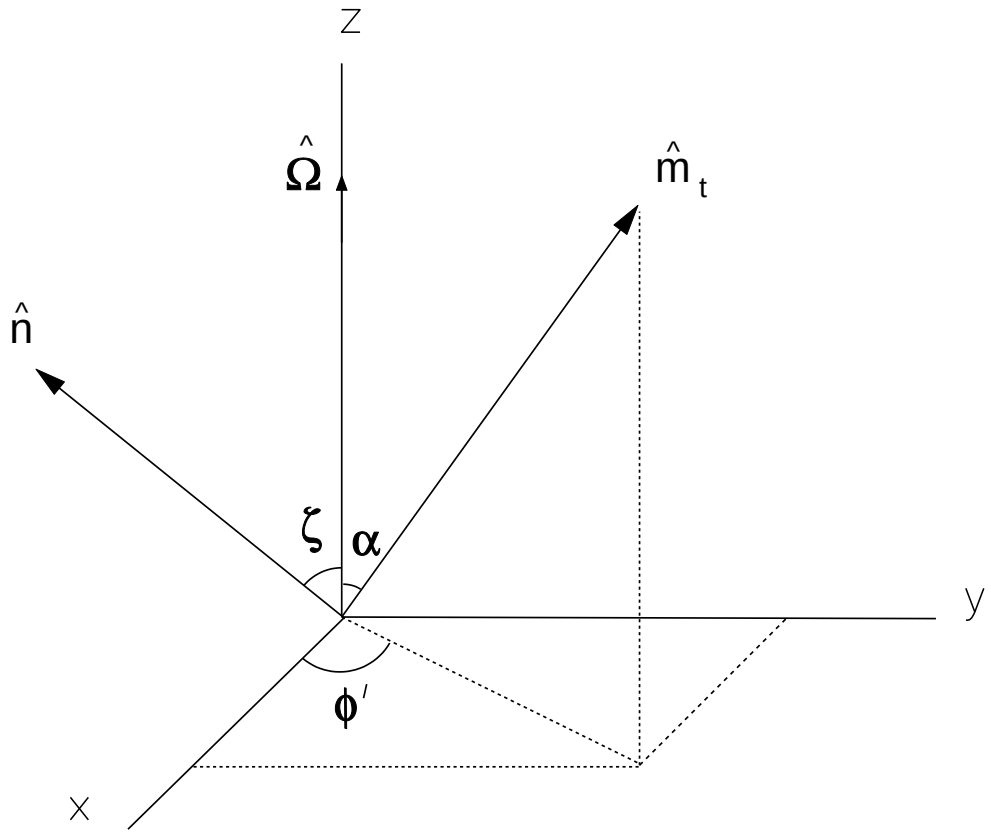

Fig. 1.— Coordinate system to describe the inclined and rotating magnetic dipole. The rotation phase ϕ' is measured from the fiducial plane (x-z) in the counter-clockwise direction around $\hat{\mathbf{\Omega}}$. The magnetic colatitude θ is measured from $\hat{\mathbf{m}}_{\rm t}$, and the magnetic azimuth ϕ measured counter-clockwise around $\hat{\mathbf{m}}_{\rm t}$ from the meridional plane defined by $\hat{\mathbf{\Omega}}$ and $\hat{\mathbf{m}}_{\rm t}$.

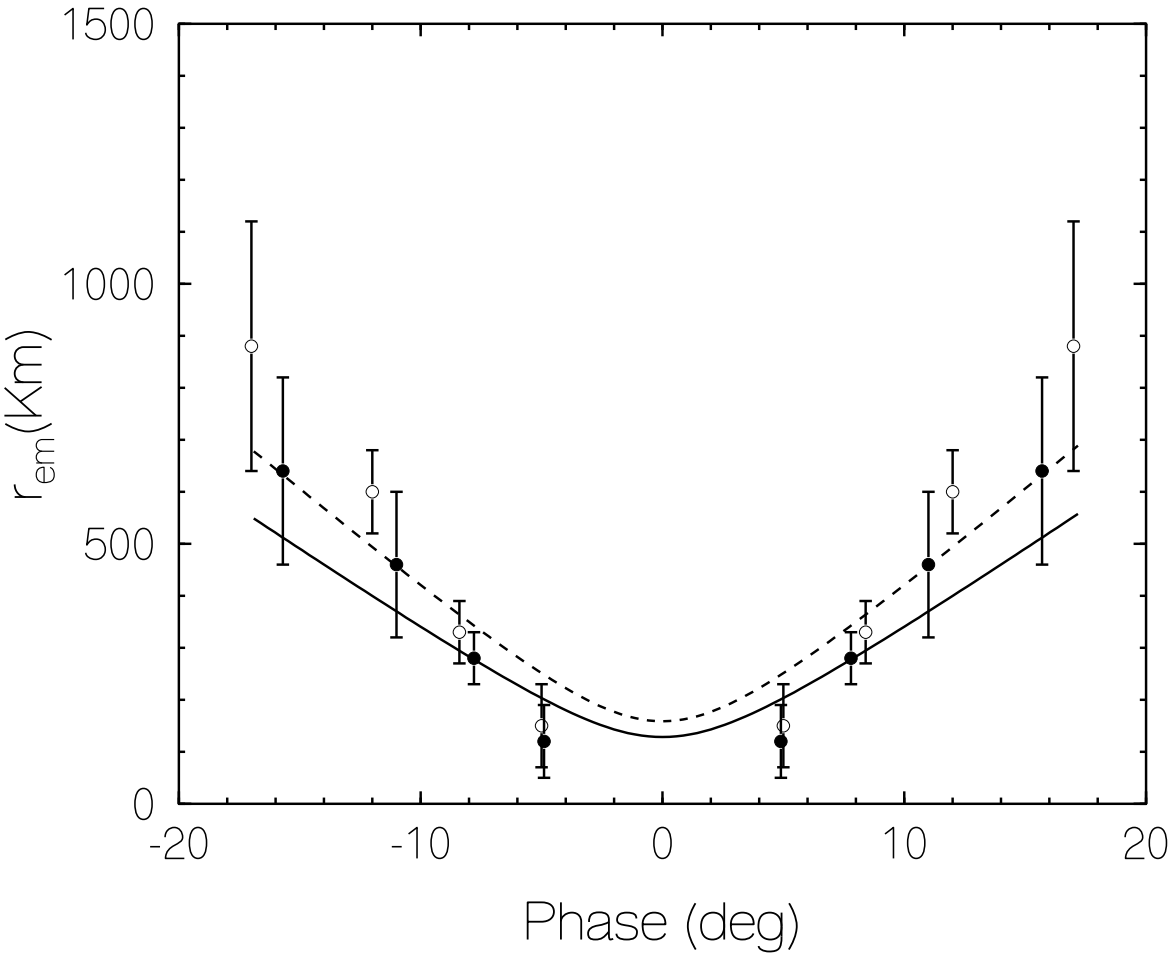

Fig. 2.— Radio wave emission heights in PSR B0329+54 with respect to rotation phase ϕ': solid and dashed line curves are for the emissions at 606 MHz and 325 MHz, respectively. The emission heights estimated from aberration-retardation phase shift (DRH03) are superposed for comparison: the points marked with ∘ and ● are for the components at 325 MHz and 606 MHz, respectively.

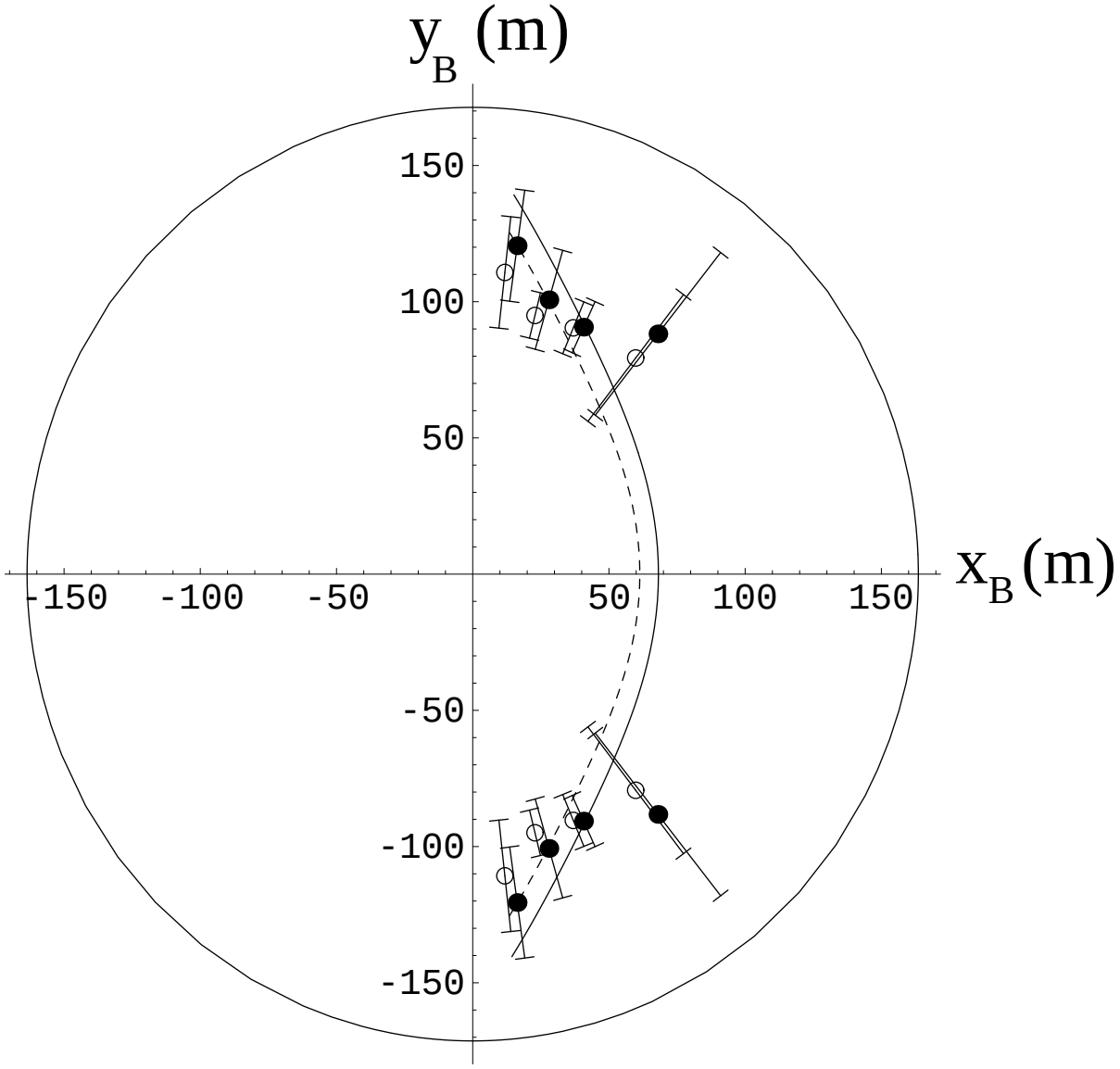

Fig. 3.— Polar cap of PSR B0329+54. Solid and dashed line curves represent the locus of foot of field lines associated with the emissions at 606 MHz and 325 MHz, respectively. The values of $s_{\rm em}$ estimated from aberration-retardation phase shift are superposed for comparison: the points marked with ∘ and ● are for 325 MHz and 606 MHz, respectively.